MODEL APERTURE IMAGING OF GAMMA-RAYS USING MULTIPLE PINHOLE ARRAYS AND MULTIWIRE PROPORTIONAL CHAMBER DETECTOR*

L. T. Chang, B. Macdonald, V. Perez-Mendez, and I. Shirakami

Lawrence Berkeley Laboratory
University of California
Berkeley, California

Abstract

Model shadows of gamma-ray distributions have been made using both random pinhole and non-redundant pinhole coded apertures with a multiwire proportional chamber as detector. Image reconstruction is done optically with incoherent light. Lateral and depth resolution results are presented and calculations of background and signal to noise ratio for the non-redundant aperture are made and compared with the single pinhole collimator.

Introduction

The pinhole collimator and the parallel hole collimator have for some time been the principal methods available for making images of distributions of gamma-ray sources in Nuclear Medicine applications. These collimators generally have a low transmission from the object to the detector (~10⁻⁴) and the images formed are necessarily a two-dimensional projection of the object. Increasing the transmission of these collimators means in most cases an unacceptable worsening of the image resolution.

It only quite recently that coded apertures have been used in gamma-ray imaging in Nuclear Medicine. In this method a coded aperture, some pattern consisting of regions either transparent or opaque to gamma-rays, is placed between the gamma-ray emitting object and the position-sensitive gamma-ray detector (Fig. 1a). The object makes a coded shadow of the aperture on the detector and this coded shadow is then decoded to produce the image. The coded aperture generally has a much larger transmission area than the single pinhole collimator which has the same resolution and it collects a correspondingly larger number of gamma-rays from the object. In addition the coded shadow contains depth information about the object since a point in the object closer to the aperture casts a larger shadow than one further away.

The first use of a coded aperture was by Mertz and Young who used an off-axis Fresnel zone plate to image X-ray stars.[1] Decoding was done by using coherent light from a laser. Barrett later applied this method to Nuclear Medicine imaging using a lead grid in front of the object to reduce the background associated with coded aperture imaging and enabling continuous distributions of gamma-ray sources to be imaged by the off-axis zone plate.[2] A coded aperture consisting of a number of pinholes randomly placed, having an average transmission of 50%, was suggested by Dicke for X-ray astronomy[3] and has been used for solar X-radiation.[4] Image reconstruction, as suggested by Dicke and also used in the work reported here, uses a mask, similar to the original coded aperture, placed between the image plane and the coded shadow which has been illuminated by a diffuse incoherent light source (Fig. 1b).

The principal coded aperture used in Nuclear Medicine imaging has been the Fresnel zone plate. This aperture has a much larger area than the single pinhole collimator which gives the same resolution image. The zone plate, however, requires more counts than the pinhole to get information about an object to the same statistical accuracy. This increase in the number of counts required goes up rapidly as the number of resolution elements in the object increases.[5,6] For an object having only a moderate number of picture elements (~200), depending on the zone plate, the zone plate collects statistical information about the object at the same rate that the single pinhole does although the event rate may be several thousand times higher. With electronic detectors such as the scintillation camera or the multiwire proportional chamber this increased data rate is a severe limitation for applications such as in Nuclear Medicine where the time available to obtain an image is limited.

Multiple pinhole coded apertures share with the zone plate the important property of being able to give three dimensional images. Their information rate can often be the same as for a zone plate while their event rate is two orders of magnitude smaller. The small number of holes (11-19) and the low total transmission of these arrays, ~1% compared to 47% for a zone plate, mean a much lower background in the image.

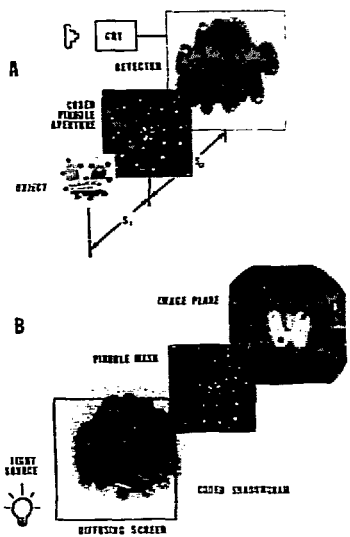

Fig. 1. Coded aperture imaging. a) Object shadowgram of Picker Thyroid Phantom using 19-hole non-redundant aperture. b) Image reconstruction from the shadowgram.

* This work has been supported by the U.S. Atomic Energy Commission and by the National Institute of General Medical Services of the National Institutes of Health, Fellowship #1F03GM57292-01 and Grant #2R01GM17147.

Properties of Multiple Pinhole Coded Apertures

Image Reconstruction and the Autocorrelation Function

The response to a point source of the multiple pinhole array coded aperture can be seen in Fig. 2.

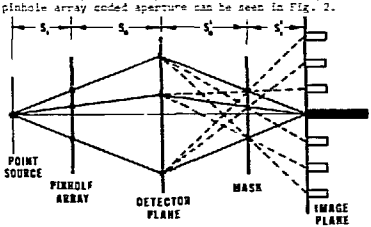

Fig. 2. Point-source response for 3-hole non-redundant aperture. Dotted lines are background.

Gamma-rays from the point source cast a magnified shadow of the aperture transmission h on the detector plane, the magnification being $m = 1 + S_0/S_1$, where S_0 is the distance between aperture and detector planes and S_1 the distance between the object and aperture planes. The center of the shadow depends on the lateral position of the source point. The shadow $s(\underline{r}')$ cast by a continuous distribution of radioactivity g in the object plane is the superposition of the shadows from each point.

$$s(\underline{r}') = \iint g(-\underline{r}\, S_1/S_0)\; h((\underline{r}'-\underline{r})/m)\; d^2\underline{r} \qquad (1)$$

This is just the convolution operation and can be written as $s = \underline{g} * h_m$, this notation showing explicitly the dependence of the coded shadow on the spatial inversion of the object- $\underline{g}(\underline{r}) \equiv g(-\underline{r})$. The shadowgram for objects in more than a single transverse plane is obtained by summing $s(\underline{r}')$ over S_1.

In reconstructing the image (right half of Fig. 2) the shadowgram $s(\underline{r}')$ in the detector plane serves as a source (of light) and the same coded aperture is used as a mask. Each point on the shadowgram casts its shadow on the image plane and, in a similar manner, the image obtained is $i = \underline{s} * h_m$, where h_m is used to show that the image plane need not be the focus of the object plane. Since $s = \underline{g} * h_m$ we have $i = (\underline{g} * h_m) * h_m = g * (h_m * h_m)$. Thus, the image we get in our two step process is equivalent to the convolution of the object with the single function a

$$i = g * a \qquad (2)$$

$$a(\underline{r}') = \iint h(\underline{r}'/m)\; h((\underline{r}'-\underline{r}')/m')\; d^2\underline{r}' \qquad (3)$$

where $a = \underline{h}_m * h_{m'}$, $m = 1 + S_0/S_1$, and $m' = 1 + S_1/S_0'$. From Eq. 2 it is seen that a is just the response of the system to a point source.

When the image plane is the focal plane for the point source, $m = m'$ and $a(\underline{r}')$ is the usual autocorrelation function of the aperture transmission h. The autocorrelation function can be obtained by superimposing on the original aperture an identical aperture displaced laterally by the distance $\underline{r}'$ and then measuring the resulting total transmission as a function of $\underline{r}'$. If the image obtained is to be recognizable without further processing it is clear from Eq. 2 that the autocorrelation function of h should have the characteristics of a delta function- a high central peak with the non-central part small and uniform.

We have investigated several multiple pinhole coded aperture arrays, shown in Fig. 3. Their autocorrelation patterns, obtained optically, are shown in Fig. 4 and, for similar types of apertures, drawn schematically in Fig. 5.

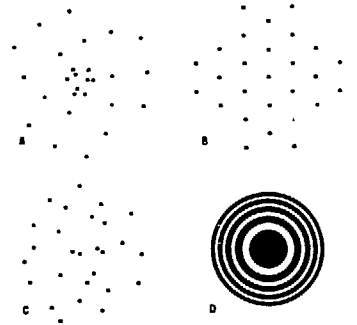

Fig. 3. Coded apertures used with wire chamber. a) Non-redundant array (27-hole) b) Redundant array (27-hole). c) Random array (27-hole) d) Fresnel zone plate

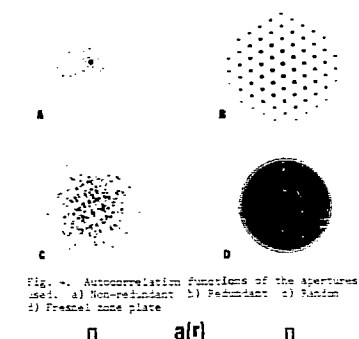

Fig. 4. Autocorrelation functions of the apertures used. a) Non-redundant b) Redundant c) Random d) Fresnel zone plate

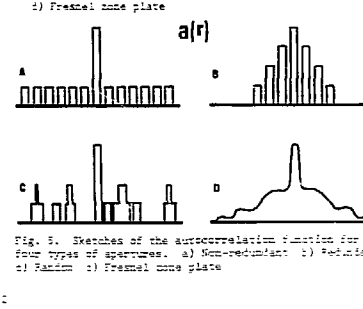

Fig. 5. Sketches of the autocorrelation function for four types of apertures. a) Non-redundant b) Redundant c) Random d) Fresnel zone plate

The N = 27 holes of Fig. 3a have been carefully located so that its autocorrelation pattern (Fig. 4a) is non-redundant. That is, while the central peak, $\underline{r}'' = 0$, has intensity N corresponding to the overlapping of all N holes from two superimposed arrays, non-central locations of $a(\underline{r}'')$ have at most intensity 1 corresponding to at most one hole from each of the superimposed arrays overlapping at a given displacement $\underline{r}''$ (Fig. 5a).

In contrast to this array, the regularly spaced array of Fig. 3b having the same number of holes has a highly redundant autocorrelation pattern (Figs. 4b and 5b). The central peak still has intensity N and the total amount of background is still the same, N(N-1), but for this array a number of holes have overlapped simultaneously giving a localized and relatively high intensity contribution to the image background. The random array (Fig. 3c), having N holes distributed randomly over the same area as the previous arrays, has an autocorrelation pattern (Figs. 4c and 5c) similar to that of the non-redundant array, its background peaks however sometimes being larger than 1. For comparison, the Fresnel zone plate coded aperture is given in Fig. 3d. Its autocorrelation function (Figs. 4d and 5d) is characterized by a high ratio (0.5) of background intensity to central peak intensity due to the high total transmission of the zone plate aperture, 50%, compared with ≈2% for the other three apertures.

By its nature the non-redundant pinhole array has the most desirable autocorrelation function and produces the lowest intensity of background in the final image. In a very different application these same non-redundant arrays, with radio telescopes replacing the pinholes, are used in astronomy for mapping radio sources. Some of these arrays are described by M. J. E. Golay.[8] Smaller non-redundant arrays (N ≤ 15) are fairly compact, that is, with most of the points of $a(\underline{r}'')$ lying within a circle with few unoccupied locations inside and only a few points lying outside. Larger arrays are built up by computer, starting with smaller ones and using various algorithms. The 27 hole pattern used here is large for a non-redundant array and less compact than many.[9]

Resolution

The lateral resolution of this imaging process depends on the size of the pinholes in the aperture and of the holes in the mask. In practice, the mask holes are made much smaller than the aperture holes and image resolution is improved, up to a factor of two better than if the holes were the same size. The smaller mask holes mean only that less light falls on the film in the reconstruction process but this just requires more incident light. In this case, the lateral resolution, expressed in object space, is just that expected for a single pinhole camera-

$$\delta_x = d\,(1 + \frac{S_0}{S_1}) \qquad (4)$$

where d is the diameter of the holes in the aperture and S_0 and S_1 are as given in Fig. 2.

The depth resolution of the imaging system can be obtained by considering the properties of the correlation function $a(g)$ (Eq. 3) when the magnification m' of reconstruction is different from the magnification m of the shadowgram produced by a point source. At point O in Fig. 6 the reconstructed image intensity is a maximum because the mask projected onto the detector plane from O completely overlaps the shadowgram of the point source. At points A or B the intensity is smaller because the projected mask pattern is either smaller or larger giving less overlap. The loss of intensity depends on the geometrical factors, S_0 and S_1, the diameter of the pinholes, and their distribution in the array. An approximate form for the depth resolution, δz, full width at half maximum in the object, is

$$\frac{\delta z}{S_1} = \frac{d}{r_a}\,(1 + \frac{S_1}{S_0}) \qquad (5)$$

where d is the diameter of the pinholes in the aperture

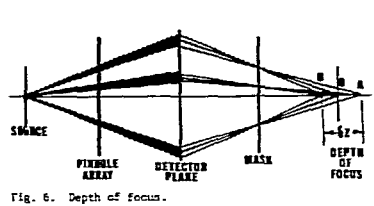

Fig. 6. Depth of focus.

and r_a is the median radius of the pinhole locations measured from the center.

Background and Noise

As we have seen, the image of a single point source using an N-hole coded aperture and incoherent reconstruction has a central intensity N corresponding to the matching of the coded shadow of the i^{th} aperture hole with the i^{th} hole in the mask for each of the N holes. Surrounding this image is background which is produced when the coded shadow of the i^{th} aperture hole combines with the j^{th} mask hole ($j \neq i$). The total amount of background for a point source is thus seen to be N(N-1) and the ratio of total background to signal intensity is just N-1, becoming worse as the number of holes in the aperture is increased. This total background can be distributed over N(N-1) points, each of intensity 1 as in the non-redundant pinhole array, or over correspondingly fewer points of higher intensity, as for the redundant array (Fig. 5c). The amount of background present with a 15-hole non-redundant array may be seen in Fig. 7 which shows the image of a thyroid phantom produced by computer calculation.

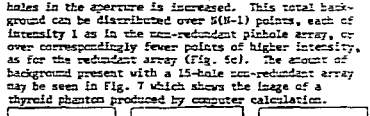

Fig. 7. Computer-generated imaging showing background. a) Thyroid phantom object b) Shadowgram from 15-hole non-redundant array c) Image, showing background

Background and statistical noise for non-redundant pinhole coded apertures can be calculated with the following assumptions--- (1) The object lies in a single transverse plane and consists of M point sources of equal intensities n_0 where n_0 is the number of detected gamma ray events which pass through one of the N aperture holes. The point sources are located on an equilateral triangular grid with separation given by the resolution length δx (Eq. 4). A triangular grid is used because our non-redundant arrays are composed on such a grid to make them more compact.
(2) The autocorrelation function is approximated by a spike of intensity N surrounded by a disc of radius r_a and intensity 1. r_a is chosen so as to contain the same number of background points, N(N-1), as does the exact autocorrelation function but packed tightly on the triangular grid. Thus, the approximate function is just a compact version of the exact function.
(3) The pinhole diameters are equal to the minimum spacing between holes in the array. This is the least resolution usable with a given non-redundant array.

The image obtained in the double process of shadowgram exposure and incoherent reconstruction is equivalent to the single step $i = o * a$. In order to provide a common scale we express the convolution in the detector plane (Fig. 2) by projecting the object through a point in the center of the aperture plane onto the

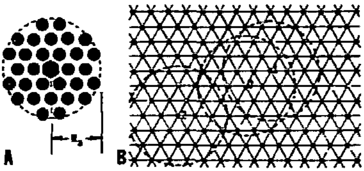

Fig. 8. Analysis of image using the autocorrelation function. a) Sketch of approximate autocorrelation function of 6-hole non-redundant array as measured in the detector plane b) Object points, spaced by the system resolution, projected onto the detector plane

detector plane. This has been done in Fig. 8. Assumption 3 assures that the spacing of the object points (Fig. 8b) is the same as the spacing of the autocorrelation points (Fig. 8a). The convolution is performed by centering the autocorrelation function on each object point and summing the results over the M object points. The signal at the center point 0 of the object has a value Nn_0. This signal is superimposed on a background B at point 0 due to the overlapping of the autocorrelation functions from neighboring object points. Those neighboring points, such as 1 in Fig. 8b which are closer than the distance r_a, each contribute $1n_0$ to the background intensity at 0. Those which are farther away than r_a, such as point 2, contribute nothing to the background at 0 since the autocorrelation function is assumed zero outside r_a. Since a maximum of N(N-1) points occur in the autocorrelation function and therefore lie within the distance r_a of the central point we have the following equations for the intensity of background at the center of the image depending on whether the actual number of object points M is greater than N(N-1) or not.

$$B = Mn_0 \qquad \text{if} \quad M \le N(N-1)$$
$$B = N(N-1)n_0 \qquad \text{if} \quad M > N(N-1) \qquad (6)$$

The background is maximum in the center of the image of our uniform object and falls to some finite value on its edges.

Noise σ in the image is due to statistical fluctuations in the number n_0 of gamma ray events and comes from independent fluctuations in the signal and in the background. Thus we have

$$\sigma = \sqrt{N+M}\sqrt{n_0} \qquad \text{if} \quad M \le N(N-1)$$
$$\sigma = N\sqrt{n_0} \qquad \text{if} \quad M > N(N-1) \qquad (7)$$

We obtain the following values for the ratio of signal to background and of signal to noise at the center of the image

$$\frac{S}{B} = \frac{N}{M} \qquad \frac{S}{\sigma} = \frac{N\sqrt{n_0}}{\sqrt{N+M}} \qquad \text{if} \quad M \le N(N-1)$$
$$\frac{S}{B} = \frac{1}{N-1} \qquad \frac{S}{\sigma} = \sqrt{n_0} \qquad \text{if} \quad M > N(N-1) \qquad (8)$$

For our N=27 hole non-redundant aperture, a relatively large number of holes, the number of object picture elements M is "large" when M > 27 x 26 = 702. The usual number of picture elements in Nuclear Medicine situations is generally larger than this number and so, in these applications, the equations for M > N(N-1) usually apply. The signal to noise ratio for a single pinhole camera is $S/\sigma = \sqrt{n_0}$ which is just what we obtain for our multi-hole aperture when M > N(N-1). Since the time is the same for both apertures to get n_0 counts/pinhole, for the same diameter pinholes, we see that for most nuclear medicine applications of non-redundant coded aperture imaging there is no net geometrical advantage over the single pinhole when producing pictures with the same resolution and the same signal to noise ratio. Fresnel zone plate coded aperture imaging is also no more efficient than the single pinhole when the number of object picture elements exceeds a certain number but this number is a function of the zone plate used.[5]

Experimental Results

The detector used in our multiple pinhole imaging was a 30 cm by 30 cm xenon-filled multiwire proportional chamber having a resolution of about 1½ mm. X-Y coordinates of gamma-ray events were determined by delay-line readout and the location of an event could be exhibited as a point of light on an oscilloscope face or digitized and read out on magnetic tape. Properties of these chambers and read-out electronics have been given elsewhere.[12] In our test objects we used gamma-rays of 30 and 60 keV energies. No attempt was made to simulate scattering by the source of the more usually employed 140 keV gamma-rays since we wished only to test the properties of the imaging system. The imaging method is applicable to the scintillation camera generally used in Nuclear Medicine giving results with somewhat less resolution.

The coded apertures used were made from 1½ mm thick lead and the arrays were usually about 8 cm across. Diameters of pinholes, 2 to 3 mm, were chosen so their shadows on the detector were at least 3 times chamber resolution.

The shadowgram transparency is made by taking time exposure of the oscilloscope which displays the gamma-ray events. Shadowgrams in coded aperture imaging are much denser in the center than on the edges and some care must be taken not to saturate the film. The developed transparency is placed on a diffusing screen and illuminated from behind, the light source being a 500 watt projector. The viewing screen is placed about a meter downstream. The mask, aluminum foil perforated with a replica of the coded aperture used, is placed between screen and shadowgram. The initial focussing is done by rotating the mask about a longitudinal axis so it lines up with the original aperture, and by moving the mask longitudinally to focus on the screen. When this is done a simple movement of the screen is all that is necessary to bring different planes in the object into focus. If the mask is made so that the ratio of mask size to film size is the same as the aperture to chamber ratio then images of different planes in the object have the same sizes.

Images of point sources taken with the apertures of Fig. 3 are shown in Fig. 9. The four point sources,

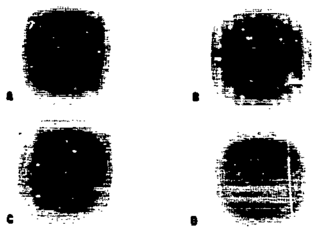

Fig. 9. Images produced by point gamma-ray sources using various apertures, with wire chamber detector and optical reconstruction. a) Non-redundant b) Redundant c) Random

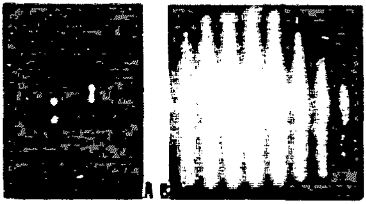

Fig. 10. Images with 27-hole non-redundant array.
a) 4 point sources, smallest spacing = 3 mm
b) Bar pattern, 3 mm bars spaced 5 mm apart

Imaged in Fig. 10a with the non-redundant array, show the system resolution is about 3 mm. These figures show no background because the biasing effect of the film used for the images eliminates the small amount of background for objects having only a few picture elements. Fig. 10b shows the response with the non-redundant aperture to a source having 5 mm bars separated by 5 mm.

A standard Picker Thyroid Phantom was used as the object and the images obtained with pinhole arrays which differ only in the placement of their 27 holes, non-redundant, redundant, and random arrays, are compared in Fig. 11. We were unable to obtain a

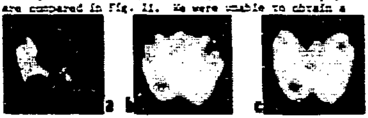

Fig. 11. Images of Picker Thyroid Phantom with 27-hole arrays. a) Non-redundant b) Redundant c) Random

recognizable image with the Fresnel zone plate aperture since its large transmission, 50%, gave a background which overwhelmed the image signal. The redundant array image is only barely recognizable because of the poor distribution of its autocorrelation function. The other two apertures, which have delta-function-like autocorrelation functions, produce good images, the non-redundant array image showing somewhat less background than that of the random array because of the less intense tails of the former's autocorrelation function. The biasing action of the film becomes apparent when the non-redundant array image is compared with the image from a similar array produced by the linear response of a computer simulation (Fig. 7).

A shadowgram was produced using sources in the shape of triangle, cross, and circle, located in 3 planes spaced 25 mm apart. Images from this shadowgram of object planes separated by 6¼ mm are shown in Fig. 12. The depth of field, calculated from Eq. 5, is 19 mm at the center.

Conclusion

Multiple pinhole array coded aperture imaging of gamma-rays has been demonstrated for three dimensional source distributions. The method can be used with a number of gamma-ray detectors with a simple optical set-up for image reconstruction.

Background is fairly low when the number N of holes is kept low but becomes larger as N increases. The distribution of background depends on the autocorrelation function of the coded aperture. Both non-redundant and random arrays give useful images but image quality is better for the former because of its smooth autocorrelation function. Background can be reduced with

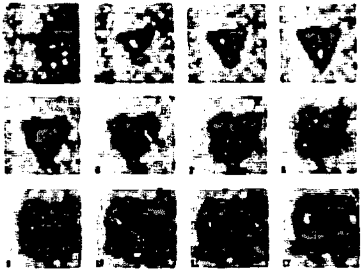

Fig. 12. Imaging of 3 objects separated in depth by 25 mm. Image planes reconstructed at intervals of 6¼ mm in the object space. 27-hole non-redundant array, S_o = 175 mm, d = 2 mm, r_m = 22 mm.
4) ▽: S_i = 100 mm, δz(calc.) = 14 mm.
8) X: S_i = 125 mm, δz(calc.) = 19 mm.
12) O: S_i = 150 mm, δz(calc.) = 25 mm.

computer processing.

Although both non-redundant and Fresnel zone plate apertures have larger areas than a single pinhole collimator of the same resolution both apertures collect information about an object no faster than the single pinhole when the number of object picture elements exceeds some number, dependent on the aperture. This number is $\approx N^2$ for the non-redundant aperture. While there are many cases in Nuclear Medicine when coded apertures are not more efficient than the single pinhole they provide depth information which the pinhole cannot. The data rate for the multiple pinhole apertures can be several hundred times smaller than for the zone plate, a distinct advantage for electronic detectors and computer information storage.

References

1. L. Mertz and N.O. Young, Proc.Int.Conf. on Opt.Inst., London, 305(1961).
2. H.H. Barrett and F.A. Horrigan, Appl. Opt. 12, 2686 (1973).
3. R.H. Dicke, Astrophysical J. 153, L101 (1968).
4. R.L. Blake, A.J. Burek, E. Fenimore, and R. Puetter, Rev. Sci. Inst. 45, 513 (1974).
5. H.H. Barrett and G.D. DeMeester, Appl. Opt. 13, 1100 (1974).
6. B. Macdonald, L.T. Chang, V. Perez-Mendez, and L. Shiraishi, IEEE Trans. Nucl. Sci. NS-21, 678 (1974).
7. A. Wouters, K.M. Simon, and J.G. Hirschberg, Appl. Opt. 12, 1871 (1973).
8. M.J.E. Golay, J.O.S.A. 61, 272 (1971).
9. W.A. Klemperer, "RADAR, Present and Future," London, 74 (1973).
10. E. Kaplan, V. Perez-Mendez, L. Kaufman, and A. Valentine, Nucl.Inst. & Meth. 106, 397 (1973).